



## A renewed rise in global HCFC-141b emissions between 2017–2021

Luke M. Western<sup>1,2</sup>, Alison L. Redington<sup>3</sup>, Alistair J. Manning<sup>3</sup>, Cathy M. Trudinger<sup>4</sup>, Lei Hu<sup>1,5</sup>,  
Stephan Henne<sup>6</sup>, Xuekun Fang<sup>7</sup>, Lambert J. M. Kuijpers<sup>8</sup>, Christina Theodoridi<sup>9</sup>, David S. Godwin<sup>10</sup>,  
Jgor Arduini<sup>11</sup>, Bronwyn Dunse<sup>4</sup>, Andreas Engel<sup>12</sup>, Paul J. Fraser<sup>4</sup>, Christina M. Harth<sup>13</sup>,  
Paul B. Krummel<sup>4</sup>, Michela Maione<sup>11</sup>, Jens Mühle<sup>13</sup>, Simon O’Doherty<sup>2</sup>, Hyeri Park<sup>14</sup>,  
Sunyoung Park<sup>14</sup>, Stefan Reimann<sup>6</sup>, Peter K. Salameh<sup>13</sup>, Daniel Say<sup>2</sup>, Roland Schmidt<sup>13</sup>,  
Tanja Schuck<sup>12</sup>, Carolina Siso<sup>1,5</sup>, Kieran M. Stanley<sup>12</sup>, Isaac Vimont<sup>1,5</sup>, Martin K. Vollmer<sup>6</sup>,  
Dickon Young<sup>2</sup>, Ronald G. Prinn<sup>15</sup>, Ray F. Weiss<sup>13</sup>, Stephen A. Montzka<sup>1</sup>, and Matthew Rigby<sup>2</sup>

<sup>1</sup>Global Monitoring Laboratory, National Oceanic and Atmospheric Administration, Boulder, CO, USA

<sup>2</sup>School of Chemistry, University of Bristol, Bristol, UK

<sup>3</sup>Hadley Centre, Met Office, Exeter, UK

<sup>4</sup>Climate Science Centre, CSIRO Oceans and Atmosphere, Aspendale, Victoria, Australia

<sup>5</sup>Cooperative Institute for Research in Environmental Sciences, University of Colorado, Boulder, CO, USA

<sup>6</sup>Empa, Swiss Federal Laboratories for Materials Science and Technology, Dübendorf, Switzerland

<sup>7</sup>College of Environmental and Resource Sciences, Zhejiang University, Hangzhou, Zhejiang, China

<sup>8</sup>A/gent b.v. Consultancy, Venlo, Netherlands

<sup>9</sup>Natural Resources Defense Council, Washington, DC, USA

<sup>10</sup>Stratospheric Protection Division, Environmental Protection Agency, Washington, DC, USA

<sup>11</sup>Department of Pure and Applied Sciences, University of Urbino, Urbino, Italy

<sup>12</sup>Institute for Atmospheric and Environmental Science, Goethe University Frankfurt,  
Frankfurt am Main, Germany

<sup>13</sup>Scripps Institution of Oceanography, University of California San Diego, La Jolla, CA, USA

<sup>14</sup>Department of Oceanography, Kyungpook National University, Daegu, Republic of Korea

<sup>15</sup>Center for Global Change Science, Massachusetts Institute of Technology, Cambridge, MA, USA

**Correspondence:** Luke M. Western (luke.western@bristol.ac.uk, luke.western@noaa.gov)

Received: 20 April 2022 – Discussion started: 27 April 2022

Revised: 21 June 2022 – Accepted: 7 July 2022 – Published: 28 July 2022

**Abstract.** Global emissions of the ozone-depleting gas HCFC-141b (1,1-dichloro-1-fluoroethane, CH<sub>3</sub>CCl<sub>2</sub>F) derived from measurements of atmospheric mole fractions increased between 2017 and 2021 despite a fall in reported production and consumption of HCFC-141b for dispersive uses. HCFC-141b is a controlled substance under the Montreal Protocol, and its phase-out is currently underway, after a peak in reported consumption and production in developing (Article 5) countries in 2013. If reported production and consumption are correct, our study suggests that the 2017–2021 rise is due to an increase in emissions from the bank when appliances containing HCFC-141b reach the end of their life, or from production of HCFC-141b not reported for dispersive uses. Regional emissions have been estimated between 2017–2020 for all regions where measurements have sufficient sensitivity to emissions. This includes the regions of northwestern Europe, east Asia, the United States and Australia, where emissions decreased by a total of  $2.3 \pm 4.6 \text{ Gg yr}^{-1}$ , compared to a mean global increase of  $3.0 \pm 1.2 \text{ Gg yr}^{-1}$  over the same period. Collectively these regions only account for around 30 % of global emissions in 2020. We are not able to pinpoint the source regions or specific activities responsible for the recent global emission rise.

## 1 Introduction

The global atmosphere has seen a decline in the burden of most ozone-depleting substances since the implementation of the Montreal Protocol on Substances that Deplete the Ozone Layer (Engel and Rigby, 2019). Under the Protocol's framework, the global phase-out of production of chlorofluorocarbons (CFCs) and halons for dispersive uses was reportedly completed in 2010. The phase-out (with the exception of very small amounts for the servicing of existing equipment) of their controlled replacement gases, primarily hydrochlorofluorocarbons (HCFCs), was completed in 2020 in developed (non-Article 5) countries, whilst developing (Article 5) countries are in the process of a staged phase-out, to be completed by 2030.

Despite a global ban on CFC production for dispersive uses, recent work found unexpected emissions of CFC-11 (trichlorofluoromethane) between 2012 and 2017, likely stemming from CFC-11 produced in violation of the Montreal Protocol after 2010 (Montzka et al., 2018; Rigby et al., 2019; Montzka et al., 2021; Park et al., 2021). These studies provided evidence of renewed dispersive use of CFC-11 in eastern China, which accounted for around 60 % of the concurrent increase in global emissions. Elevated emissions from eastern China of both CFC-12 and  $\text{CCl}_4$ , chemicals involved in the production of CFC-11, from which they can escape to the atmosphere, suggested that CFC-11 production may have also occurred in this region. The most likely application of this newly produced CFC-11, which was not reported to the United Nations Environment Programme's (UNEP) Ozone Secretariat, was as a blowing agent for closed-cell foams (TEAP, 2019).

The most widely used replacement gas for CFC-11 for foam blowing in developing countries was HCFC-141b (1,1-dichloro-1-fluoroethane,  $\text{CH}_3\text{CCl}_2\text{F}$ ), which also has minor applications as an aerosol, a solvent and feedstock and is also an intermediate/by-product during the production of other fluorochemicals. Under the phase-down schedule of the Montreal Protocol, HCFC-141b should no longer be produced or consumed for dispersive uses in developed countries, and production should be declining in developing countries since the HCFC phase-out began in 2013. HCFC-141b has a much shorter atmospheric lifetime than CFC-11 (around 9.4 compared to 52 years), and its potential to deplete stratospheric ozone is only around 0.07–0.10 times that of CFC-11 (Burkholder, 2019). Yet, HCFC-141b is still an ozone-depleting substance, with the potential to delay stratospheric ozone recovery, and, along with other HCFCs, it is also a potent greenhouse gas, with a global warming potential 800 times that of carbon dioxide over a 100-year time horizon (Burkholder, 2019).

Reported global HCFC-141b consumption – defined as production for dispersive uses plus imports minus exports

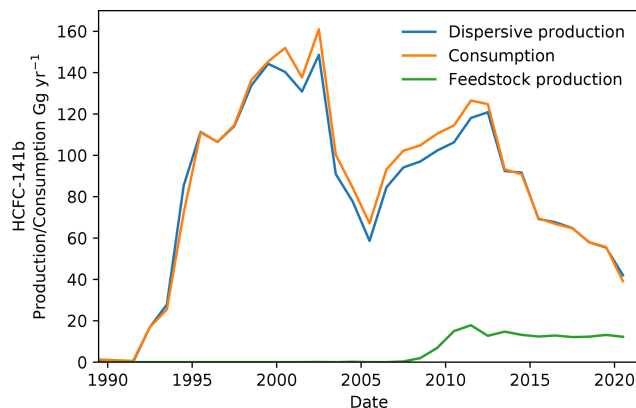


**Figure 1.** Global HCFC-141b production for dispersive uses (blue) and consumption (orange) reported to UNEP. Production of HCFC-141b for use as a feedstock (green) is not included in the reported total for dispersive production or compliance considerations with respect to the Montreal Protocol.

and destruction – exhibits two peaks (Fig. 1), one in 2002 and one in 2011. In addition to foam blowing, dispersive uses for HCFC-141b are as an aerosol (1.4 Gg was consumed for aerosols in 2014 and 0.7 Gg in 2018) and a solvent (Multilateral Fund, 2019). The use of HCFC-141b for solvent cleaning has declined, from 4.7 in 2014 to 3.8 Gg yr<sup>-1</sup> in 2018 and is predicted to decline further (MCTOC, 2018; Multilateral Fund, 2019). HCFC-141b produced for use as a feedstock is differentiated from dispersive production when reported as its production quantity is not relevant for compliance with the Montreal Protocol due to an earlier, but incorrect, assumption of negligible emissions from feedstock production and use (production for both dispersive uses and feedstock is shown in Fig. 1). Production of HCFC-141b for feedstock was at a maximum of 18 Gg yr<sup>-1</sup> in 2011, compared to 118 Gg yr<sup>-1</sup> in 2011 for dispersive uses, and has remained at 12–13 Gg yr<sup>-1</sup> between 2014–2020. However, the proportion of HCFC-141b produced as feedstock increased from 12 % in 2014 to 23 % in 2020 due to the decline in production for dispersive uses. HCFC-141b can be a feedstock, a by-product and a target product. Starting out from methyl chloroform or vinylidene chloride (VDC), HCFC-141b, HCFC-142b and HFC-143a are produced (Andersen et al., 2021). HCFC-142b can then be converted to vinylidene fluoride (VDF, HFO-1132a), a refrigerant and also the building block for the fluoropolymer polyvinylidene fluoride (PVDF). Any unwanted HCFC-141b can also be fed into this production chain (TEAP, 2021; Andersen et al., 2021). While the size and exact fate of these production routes are not publicly known, it is possible that the market for PVDF is growing due to its use in Li-ion batteries and other high-tech applications. Previous estimates of global HCFC-141b emissions, last reported up to 2016, based on atmospheric

observations have generally been consistent with inventory estimates, based on consumption reported to UNEP (neglecting feedstock) and assumptions about rates of release to the atmosphere (Montzka et al., 2015; Simmonds et al., 2017; Engel and Rigby, 2019).

Regional top-down (based on atmospheric measurements) and bottom-up (based on assumptions about the size and rate of release from various emissive processes and reported or market-based estimates) HCFC-141b emission estimates are sparse and exist only for northeast Asia, India, western Europe and the United States. Top-down emissions estimates for China through 2017 by Fang et al. (2019b) show emissions declining from  $24 \pm 5$  to  $15 \pm 2$  Gg yr<sup>-1</sup> between 2011 and 2017. A decline in Chinese emissions in recent years is supported using a different set of atmospheric data by the estimates of Yi et al. (2021), albeit with smaller overall emissions, showing Chinese emissions peaking at 16 Gg yr<sup>-1</sup> in 2014 and dropping to 11 Gg yr<sup>-1</sup> by 2019 (uncertainties were not given). Conversely, bottom-up estimates for China projected a peak in emissions in 2018 (26 Gg yr<sup>-1</sup>) (Wan et al., 2009) or the mid-2020s (31 to 35 Gg yr<sup>-1</sup>) (Wang et al., 2015; Fang et al., 2018), when foam products come to the end of their life following peak consumption. The refrigeration and electric water-heater sectors contribute most significantly to these disposal-related emissions (Wang et al., 2015). Statistics on China's refrigerator production and disposal projected a continued increase in HCFC-141b emissions from China into 2020, when emissions were estimated to be around 12 Gg yr<sup>-1</sup> from household refrigerator disposal (Zhao et al., 2011). Top-down emissions estimates for India based on measurements from an aircraft campaign in June–July 2016 were 1.0 (0.7–1.5) Gg yr<sup>-1</sup> (Say et al., 2019), while estimates for Europe from 2009 are estimated to be in the region of 1.4 (0.8–2.0) Gg yr<sup>-1</sup> (Keller et al., 2012). Bottom-up estimates for the United States by the U.S. Environmental Protection Agency (EPA) (EPA, 2021) reached a maximum of 9.1 Gg yr<sup>-1</sup> in 2014 and declined to 7.1 Gg yr<sup>-1</sup> in 2017, with a slowing rate of decline to 6.7 Gg yr<sup>-1</sup> in 2020. The reason for the peak in US emissions following a long-term decline in consumption is likely due to an increase in emissions at the end of life of rigid boardstock, commercial refrigeration foams and domestic refrigerator–freezer insulation products.

This work explores whether an increase in global HCFC-141b emissions, starting in 2018, can be fully attributed to emissions from the HCFC-141b bank due to dispersive production reported to UNEP, or from other activities that may not be reported under the Montreal Protocol. Next, we present overviews of the data sets and modelling approaches used in Sect. 2. We then present estimates of global HCFC-141b emissions based on atmospheric measurements and reported consumption (Sect. 3.1) and regional emission estimates for east Asia (Sect. 3.2), Europe (Sect. 3.3), the United States (Sect. 3.4) and Australia (Sect. 3.5), followed by the conclusions (Sect. 4).

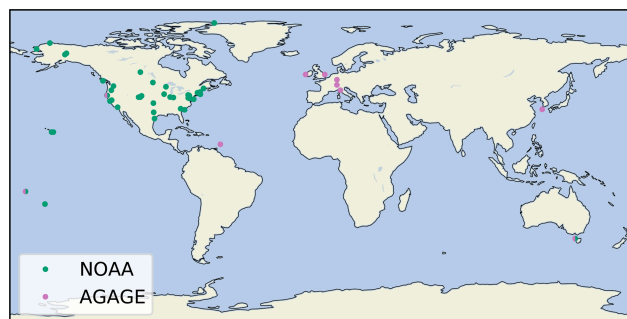


**Figure 2.** Locations of the AGAGE (pink circles) and NOAA (green circles) measurement stations used in this work to estimate global and regional HCFC-141b emissions.

## 2 Methods

### 2.1 Measurements

We use measurements of dry-air atmospheric mole fractions from two global monitoring networks, the Advanced Global Atmospheric Gases Experiment (AGAGE, Prinn et al., 2018) and the United States National Oceanic and Atmospheric Administration (NOAA) Global Greenhouse Gas Reference Network (Montzka et al., 2015; Hu et al., 2015, 2016, 2017). Measurements from AGAGE and NOAA stations in the remote atmosphere were used separately to estimate global emissions. Measurements from AGAGE stations provide regional emissions estimates for Europe, Australia and east Asia and NOAA stations for the United States. Figure 2 shows the locations of the measurement stations, and further information is summarised in Tables S1 and S2.

AGAGE HCFC-141b measurements are reported on the Scripps Institution of Oceanography (SIO) 2005 calibration scale. The Medusa GC–MS instruments in Table S1 are cryogenic pre-concentration systems coupled with a gas chromatograph (GC, Agilent) and quadrupole mass selective detector (MSD) (Miller et al., 2008; Arnold et al., 2012). The ADS–GC–MS is an adsorption–desorption system with a gas chromatograph and mass spectrometer (Maione et al., 2013). AGAGE in situ atmospheric measurements were made with these systems approximately every 2 h (Medusa GC–MS) or 4 h (ADS–GC–MS). Paired flask samples were collected at the Taunus observatory (Table S1) and analysed on a GC–quadrupole MSD (Schuck et al., 2018). Before in situ measurements were available (1994 in the Northern Hemisphere and 1998 in the Southern Hemisphere), global emission estimates are based on archived air samples (historic air samples collected and stored). Archived air samples from the Cape Grim Air Archive (CGAA, collected 1978–2009) for the Southern Hemisphere were measured in 2011 using Medusa GC–MS technology, also on the SIO-2005 scale (Fraser et al., 2018). Several CGAA and 126 archived air samples taken at Trinidad Head and other locations in the Northern Hemisphere between 1973–2016 were measured at

the Scripps Institution of Oceanography using Medusa GC–MS technology (Mühle et al., 2010; Trudinger et al., 2016; Mühle et al., 2019). These archived air samples can therefore be easily integrated with the later AGAGE in situ measurements.

NOAA estimates of the global mean, remote atmospheric abundance of HCFC-141b considered here are derived from measurements of air samples pressurised into paired stainless-steel flasks that have been collected approximately weekly at eight remote sites since the earlier 1990s (see Table S2). The flasks are shipped to Boulder for analysis on customised GC–MS instruments (Montzka et al., 2015). For deriving continental US emissions from atmospheric measurements, additional flask samples are regularly collected from tall towers (100–400 m a.g.l.; a single flask per sample, typically) and as profiles from aircraft (6 to 12 flasks collected at regular altitude intervals in a profile up to 8 km a.s.l.) at 17 profiling locations (Hu et al., 2017).

## 2.2 Global emission modelling

### 2.2.1 Measurement-based global emissions inference

Global top-down emissions of HCFC-141b, and inferred global mole fractions, are estimated based on atmospheric mole fraction measurements from either the AGAGE or NOAA network, a 12-box model of global transport and inverse modelling. The 12-box model simulates annually repeating advection and diffusion in the global atmosphere (Cunnold et al., 1983; Rigby et al., 2013) and separates the atmosphere at 30° N, the Equator and 30° S and at 500 and 200 hPa. The rate of reaction of HCFC-141b with the hydroxyl radical (OH) was taken from Burkholder (2019), and global mean OH concentrations were inferred in the box model based on observations of methyl chloroform (Rigby et al., 2013). A first-order stratospheric loss was imposed to give a stratospheric lifetime of 72.3 years. The overall lifetime of HCFC-141b was 9.3 years in the model.

The measurements from the AGAGE sites that are representative of background conditions in the semi-hemispheres of the 12-box model are used to estimate global emissions (MHD, THD, RPB, SMO and CGO; see Table S1) after measurements not representative of background conditions were removed using a statistical algorithm (O’Doherty et al., 2001). When measurements are made in the same latitude band using multiple instruments (MHD and THD), the mean value is used. AGAGE monthly mean estimates are based on one to a few archived air measurements or dozens to hundreds of in situ measurements. NOAA measurements used as input to the 12-box model are shown in Table S2. They were also filtered to select only those thought to be representative of background conditions, eliminating a small fraction of the entire data record (1.7 % of flask pairs). Results were also eliminated when measured mole fractions in simultaneously filled flasks differ by more than 0.28 ppt (3.0 % of all

flask pairs). Monthly semi-hemispheric means were derived using a cosine weighting of site latitude. See Tables S1 and S2 and Sect. 2.1 for more details on the measurement sites and instruments used.

Emissions are estimated using an inverse framework (Rigby et al., 2014), through minimisation of a cost function that constrains the emissions growth rate between years. A priori, the growth rate was assumed to be zero plus or minus 20 % of the maximum emissions from the EDGAR v4.2 bottom-up data set (Janssens-Maenhout et al., 2011). Systematic uncertainties in the inferred emissions, in addition to the measurement error, are derived using a Monte Carlo approach, which includes errors due to transport, HCFC-141b lifetime (1 standard deviation uncertainty of 15 % was assumed, based on SPARC, 2013) and instrument calibration. The mole fraction growth rate is calculated as the annual growth rate per month and is smoothed using a Kolmogorov–Zurbenko (KZ) filter (Yang and Zurbenko, 2010) using an approximately 18-month window.

### 2.2.2 Consumption-based global emissions modelling

We estimate emissions using reported global consumption data and an adaptation of the methodology employed by Simmonds et al. (2017), where release rates from the reported bank are estimated to best reproduce the top-down global emissions estimates. We call this approach a top-down-informed bank model. In a given year,  $i$ , total emissions to the atmosphere,  $E$ , are assumed to come from a combination of prompt releases in the year of consumption,  $C$  (due to losses during production and installation), and emissions from the existing HCFC-141b bank,  $B$ , following the relationship

$$E_i = fC_i + gB_i, \quad (1)$$

where  $f$  and  $g$  are the prompt and bank release fractions, respectively, and remain constant over time. The bank grows as

$$B_i = (1 - f)C_{i-1} + (1 - g)B_{i-1}. \quad (2)$$

We extend this approach by using separate consumption data for Article 5 and non-Article 5 countries, each with very different consumption patterns over time, which allows each to have their own prompt and bank release fractions (rather than the same release fraction, as used in Simmonds et al., 2017).

To derive values for  $f$  and  $g$  for both Article 5 and non-Article 5 countries, we use the top-down global emissions estimates and a statistical framework. For this analysis, we only use emissions estimated using AGAGE data, as this measurement data set includes measurements of archived air samples, which predate the non-negligible global consumption, whereas the NOAA data do not. We constrain  $f$  and  $g$  using the top-down emissions and the relationship in Eq. (1) in a Markov chain Monte Carlo framework, which allows uncertainties to be propagated throughout. No prior constraint is

placed on the value of  $f$  and  $g$ , other than that they must be between 0%–100% with equal prior probability. Under this framework, we simultaneously infer consumption in 2021, which had not been fully reported to UNEP at the time of writing, considering the uncertainties in the top-down emissions and release fractions. For 2021, we assume that all consumption from non-Article 5 countries is less than  $1 \text{ Gg yr}^{-1}$  (with equal probability for all values between  $0\text{--}1 \text{ Gg yr}^{-1}$ ) and place no prior constraint on Article 5 consumption, other than it must be a positive value. We make this assumption as, under the phase-out schedule, only very minor consumption (less than 0.5% of baseline usage, which is around  $0.2 \text{ ODP-Gg}$  for all HCFCs, where  $\text{ODP-Gg}$  is the CFC-11 equivalent in terms of ozone-depleting potential) would be expected from non-Article 5 countries. Consumption of HCFC-141b in 2020 for non-Article 5 countries was negative; i.e. more HCFC-141b was destroyed than consumed. Therefore, it is reasonable to assume that any consumption, above minor usage, should only occur in Article 5 countries. As such, it is possible to use the estimated 2021 consumption and estimates of release fraction to predict 2021 emissions (with the propagated uncertainty).

### 2.3 Regional modelling

Regional emission estimates for east Asia were derived using four inverse methods: the Bristol Markov chain Monte Carlo (MCMC) inversion, Sect. 2.3.1; InTEM, Sect. 2.3.2; EBRIS, Sect. 2.3.3; and FLEXPART-MIT, Sect. 2.3.4. Regional emissions for northwest Europe (NW Europe) and Australia were derived using InTEM, Sect. 2.3.2. Regional emissions for the contiguous United States were derived using the NOAA framework, Sect. 2.3.5. Inverse methods were run with independent choices to a priori emissions, statistical models, transport set-ups and treatment of measurement data sets, in instances where multiple estimates were performed for the same region.

#### 2.3.1 Bristol MCMC

Linear sensitivities of measured mole fraction to emissions (or “footprints”) were derived using the UK Met Office NAME model (Jones et al., 2007). Sensitivities were calculated for a computational domain bounded at  $5^\circ \text{ S}$  and  $74^\circ \text{ N}$  and  $55$  and  $192^\circ \text{ E}$ . Meteorology from the UK Met Office Unified Model (Met-UM Global, Walters et al., 2014) drives the transport, which increases in resolution from  $0.563$  to  $0.141^\circ$  longitude and  $0.375$  to  $0.094^\circ$  latitude between 2008–2020. The temporal resolution remained at 3 h throughout this period. Around 20 000 particles were released each hour within the NAME model domain, and a measurement was deemed to be sensitive to emissions when a particle was transported within the lowest 40 m above ground level of the model domain. Sensitivities were output on a grid of  $0.234^\circ$  longitude by  $0.352^\circ$  latitude.

Emissions were estimated using a Bayesian Markov chain Monte Carlo inverse framework (Ganesan et al., 2014; Say et al., 2019) independently each year by scaling an a priori emissions field and the mole fraction contribution from the model boundary using measurements from Gosan station averaged into 12-hourly bins. The a priori emissions field is  $1.16 \text{ Gg yr}^{-1}$  for eastern China,  $0.13 \text{ Gg yr}^{-1}$  for South Korea,  $0.17 \text{ Gg yr}^{-1}$  for western Japan and  $0.17 \text{ Gg yr}^{-1}$  for North Korea. Emissions were distributed equally in space over land with a log-normal uncertainty, where the distribution is described by the shape parameters  $\mu$ , or log-median value, equal to 0.2, and  $\sigma$ , equal to 0.8. The a priori mole fraction at the model boundary was taken from the AGAGE 12-box model (Rigby et al., 2014). These were assigned a prior log-normal distribution, with  $\mu$  equal to 0.004 and  $\sigma$  equal to 0.02. In addition to the measurement error, which was assumed prior to inference, we estimated the model transport error in a normal likelihood, assigning it a log-normal prior distribution of  $\mu$  equal to 0.2 and  $\sigma$  equal to 0.8. The computational domain was divided into 151 basis functions using a quadtree algorithm, and the mole fractions at the boundaries were estimated in each cardinal direction (Say et al., 2019; Western et al., 2021). We used a No-U-Turn (NUTS) sampler to sample the emissions and boundary influence and a slice sampler to sample the model error (Salvatier et al., 2016) using 90 000 sampling steps (with an additional 10 000 discarded at the beginning of the sampling chain). Convergence was checked using a Gelman–Rubin diagnostic (Gelman and Rubin, 1992) on multiple chains.

#### 2.3.2 InTEM

The InTEM inversion methodology is described in Manning et al. (2021). Briefly, the footprint sensitivities were generated using NAME as described in Sect. 2.3.1 using global UM data. Emission estimates for east Asia were derived using measurement data from Gosan, averaged into 4-hourly time intervals. Prior mean emissions in east Asia were uniformly distributed over all land areas within the computational domain, with total emissions equal to  $50 \text{ Gg yr}^{-1}$  and a 1 standard deviation uncertainty equal to 300% of the prior mean emissions. This resulted in the following prior emissions: eastern China  $2.6 \pm 24.3 \text{ Gg yr}^{-1}$ , South Korea  $0.3 \pm 8.7 \text{ Gg yr}^{-1}$ , western Japan  $0.4 \pm 9.9 \text{ Gg yr}^{-1}$  and North Korea  $0.4 \pm 9.0 \text{ Gg yr}^{-1}$ .

Emission estimates for Europe used measurement data from Mace Head, Jungfraujoch, Monte Cimone, Tacolneston and Taunus. For Europe, the footprints were bounded by a computational domain of  $10.6$  to  $79.2^\circ \text{ N}$ ,  $98.1^\circ \text{ W}$  to  $39.6^\circ \text{ E}$  using global UM data nested with higher-resolution Unified Model meteorology over the United Kingdom and Ireland (UK-V, Tang et al., 2013). The prior emissions for countries in NW Europe were  $0.1 \pm 4.4 \text{ Gg yr}^{-1}$  for Belgium and Luxembourg,  $1.8 \pm 18.1 \text{ Gg yr}^{-1}$  for France,  $1.1 \pm 13.5 \text{ Gg yr}^{-1}$  for Germany,  $0.3 \pm 6.8 \text{ Gg yr}^{-1}$

for Ireland,  $0.1 \pm 4.8 \text{ Gg yr}^{-1}$  for the Netherlands and  $1.1 \pm 12.7 \text{ Gg yr}^{-1}$  for the UK.

Emissions estimates for Victoria, Tasmania, southern and southwestern New South Wales, and eastern South Australia are based on measurements at Cape Grim, averaged every 4 h. They are then scaled by population (a factor of 2.6) to the whole of Australia. Footprints were bound to a computational domain of  $70.0$  to  $214.7^\circ \text{ E}$  and  $65.0^\circ \text{ S}$  to  $5.0^\circ \text{ N}$ . The prior emissions for Australia were  $0.4 \pm 2.0 \text{ Gg yr}^{-1}$ , distributed by population density.

Prior boundary mole fractions at each station were estimated using a fourth-order polynomial fitted to measurements that were representative of background air, having little influence from populated areas, and refined within the In-TEM framework (see Manning et al., 2021).

### 2.3.3 EBRIS

A detailed description of the Empa Bayesian Regional Inversion System (EBRIS) is given in Henne et al. (2016). The method used measurements from the Gosan station, averaged every 3 h, to derive emissions. Footprint sensitivities for east Asia were derived using the FLEXPART transport model (Pisso et al., 2019), which was driven by operational ECMWF analysis meteorology with  $1^\circ \times 1^\circ$  resolution, reducing to  $0.2^\circ \times 0.2^\circ$  resolution for northeastern China ( $105$  to  $125^\circ \text{ E}$  and  $30$  to  $50^\circ \text{ N}$ ). In each 3 h interval, 50 000 particles were released and tracked backward for 10 d. Footprints were derived for a large northern hemispheric domain at a resolution of  $0.125^\circ \times 0.125^\circ$  and a particle sampling height of 100 m.

Inversions were carried out independently for average annual emissions. The inversion grid (state vector) was limited to the domain  $80$  to  $140^\circ \text{ E}$  and  $20$  to  $60^\circ \text{ N}$ . Grid resolution was inversely proportional to the average footprint, with smaller grid cells ( $0.125^\circ \times 0.125^\circ$ ) close to the measurement site and large grid cells ( $8^\circ \times 8^\circ$ ) away from the measurement site. Approximately 500 grid cells were included in the inversion grid, depending on the data coverage of individual years.

Baseline concentrations were estimated using the robust estimation of baseline signal (REBS) method (Ruckstuhl et al., 2012) applied to the observations at Gosan. Every 2 weeks baseline concentrations were part of the state vector and were optimised during the inversion step.

The same a priori emissions were assigned for each year in the inversion. Homogeneous a priori distributions were prescribed in each of the seven focus regions (western China,  $6.3 \text{ Gg yr}^{-1}$ ; eastern China,  $6.7 \text{ Gg yr}^{-1}$ ; North Korea,  $0.1 \text{ Gg yr}^{-1}$ ; South Korea,  $1.0 \text{ Gg yr}^{-1}$ ; western Japan,  $2.0 \text{ Gg yr}^{-1}$ ; eastern Japan,  $0.6 \text{ Gg yr}^{-1}$ ; Taiwan,  $0.2 \text{ Gg yr}^{-1}$ ).

The a priori covariance and data-mismatch covariance were estimated using a log-likelihood optimisation of parameters describing the covariance (Henne et al., 2016). As part

of this optimisation the domain total a priori uncertainty was determined to be 140 % to 160 % varying from year to year.

### 2.3.4 FLEXPART-MIT

The FLEXPART-MIT inversion is described in Fang et al. (2019a). The FLEXPART-MIT inversion also used FLEXPART to derive footprint sensitivities, but under a different setup to Sect. 2.3.3. In every 3 h interval, 40 000 particles were released and tracked backwards for 20 d. Meteorology was driven by operational ECMWF analysis at  $1^\circ \times 1^\circ$  global resolution over a global computational domain.

A priori flux fields were spatially uniform over continental eastern Asia, with no emissions from the ocean. Emissions were estimated using a variable-resolution grid. The grid was finest ( $1^\circ \times 1^\circ$ ) in eastern China and other eastern Asian countries, and a coarser grid resolution ( $24^\circ \times 24^\circ$ ) was used outside this area. A priori emissions estimates of HCFC-141b were  $14.5 \text{ Gg yr}^{-1}$  for China ( $1.5 \text{ Gg yr}^{-1}$  for eastern China) and 1.2, 0.27 and  $0.27 \text{ Gg yr}^{-1}$  for Japan, South Korea and North Korea, respectively. Prior uncertainty was arbitrarily set to 1000 % of the a priori estimate, which assumed a spatial correlation length of 300 km. The background mole fractions were estimated in 7 d periods. Model–measurement uncertainty for each 24 h averaged observation was estimated using the quadratic sum of 1 % of the baseline value (as a measure of baseline uncertainty), the measurement repeatability and the standard deviation of the 24 h variability (as a measure of the model–data mismatch uncertainty).

The inverse framework utilises a Bayesian framework using an analytical solution to a normal likelihood and prior (Stohl et al., 2009) for each year.

### 2.3.5 NOAA

The NOAA inversion framework was first presented in Hu et al. (2015) and is used to derive US emissions for a number of ozone-depleting substances and their substitutes (Hu et al., 2016, 2017). A similar methodology was used here to derive US emissions of HCFC-141b for 2015–2020. A total of six ensemble inversions with identical a priori emission fields were conducted for deriving US HCFC-141b emissions (three approaches to estimate background mole fraction using two transport models). The US a priori HCFC-141b emissions were  $4.1 \text{ Gg yr}^{-1}$  and were scaled by population density to generate  $1^\circ \times 1^\circ$  a priori emissions. Prior uncertainties were estimated by maximum likelihood estimation (Michalak et al., 2005; Hu et al., 2015). Footprints were simulated by two transport models, the Hybrid Single-Particle Lagrangian Integrated Trajectory Model (HYSPPLIT) for 2015–2020 and the Stochastic Time-Inverted Lagrangian Transport (STILT) model for 2015–2017. The HYSPPLIT model was run with 500 particles back in time for 10 d and driven by the North American Mesoscale Forecast System (NAM5) with 40 sigma-pressure levels and 12 km hor-

horizontal resolution over the contiguous United States. The NAMS meteorology was nested with a global meteorological field, the US National Centers for Environmental Prediction (NCEP) 0.5° Global Data Assimilation System (GDAS0.5) with 55 sigma-pressure levels (before June 2019) and the NCEP 0.25° Global Forecast System (GFS0.25) forecast model with 55 sigma-pressure levels (after June 2019). The STILT simulation was also run with 500 particles back in time for 10 d. It was driven by the Weather Research and Forecasting Model (WRF) with 10 km resolution over North America and 40 km resolution outside of North America.

Three different approaches were used to derive background HCFC-141b mole fractions for measurements made in the United States (see details described in Hu et al., 2017, 2021). All three approaches were first based on a 3D background field (as a function of time, latitude and altitude) constructed from atmospheric observations far away from emission sources, i.e. those made over the Pacific Ocean and Atlantic Ocean basins near Earth's surface and in the free troposphere above North America. In the first approach, we estimated the background mole fraction associated with each measurement made in the United States by assigning mole fractions from this 3D background field based on the sampling time, latitude and altitude for measurements made in the United States. In our second approach, we considered air back-trajectories for individual measurements made in the United States. We estimated the time and location of each particle exiting the planetary boundary layer of the contiguous United States based on its back-trajectories and assigned the mole fraction from the 3D background at the exiting time and location. The third background estimate for each measurement in the United States is an average of 500 background estimates based on the 500 back-trajectories. In this third approach, we considered possible biases in transport simulations and lack of mole fraction information in the planetary boundary layer of the United States, because some particles remained in the planetary boundary layer of the United States after 10 d of running the transport model backward in time. Thus, we applied a likely bias correction to the background derived from the second approach by comparing observed mole fractions with estimated background mole fractions for a subset of observations with minimal surface emission influence, i.e. summed footprint over populated areas (areas with more than 10 persons per square kilometre) less than  $0.1 \text{ ppt} (\text{pmol m}^{-2} \text{ s}^{-1})^{-1}$ . The final annual US emissions were reported as the ensemble mean and uncertainties from the six inversions. The reported uncertainties are a 1-sigma uncertainty ( $\sigma_t$ ) calculated as

$$\sigma_t = \sqrt{\sigma_s^2 + \frac{1}{6} \sum_{i=1}^6 \sigma_i^2}, \quad (3)$$

where  $\sigma_i$  is the 1-sigma posterior uncertainty derived from each inversion;  $\sigma_s$  denotes the 1-sigma spread of the posterior emissions derived from all six inversions.

### 3 Results and discussion

#### 3.1 Global mole fraction and emissions

As expected from the Montreal Protocol-mandated HCFC phase-out schedule, global emissions of HCFC-141b had been declining since 2012 (Montzka et al., 2015; Simmonds et al., 2017; Engel and Rigby, 2019). However, since 2017, an increase in emissions is evident from recent changes in the distribution and global mean mole fraction of HCFC-141b. The growth rate of the global mole fractions had continuously slowed since 2012, and the global mole fractions started to decline during 2017 (Fig. 3a and b for AGAGE and NOAA, respectively). Such a slow-down and decline are expected as emissions decrease and HCFC-141b present in the atmosphere is destroyed by reactions with the OH radical and photolysis in the stratosphere. Since 2018, however, the rate of decline in global mole fraction slowed and, as of 2019, annual mean growth rates are positive again. This increase is likely being driven by increased emissions in the Northern Hemisphere, as the increase in the growth rate in the Northern Hemisphere leads that in the Southern Hemisphere in recent years, just as it did in earlier periods when the global HCFC-141b growth rate and emissions were rapidly increasing (e.g. 1992–1996 and 2009–2012). As of 2019 there is a growing difference between the observed mole fraction in the Northern Hemisphere and Southern Hemisphere (mean difference of 1.8 ppt in 2018 and 2.2 ppt in 2021).

Using AGAGE and NOAA measurements, we show that emissions of HCFC-141b started to increase again in 2018, despite the reported reduction in global dispersive production and consumption expected from the Montreal Protocol control schedules (Figs. 1 and 4a). Aggregated emissions from 2017 to 2021 have increased by an additional  $4.4 \pm 1.9$  (AGAGE) or  $7.5 \pm 0.5$  Gg (NOAA), an average linear increase at a rate of  $1.1 \pm 0.2 \text{ Gg yr}^{-1}$  per year (AGAGE) or  $1.6 \pm 0.1 \text{ Gg yr}^{-1}$  per year (NOAA). This assumes that all uncertainty is only due to the random error component of the emissions estimates (i.e. systematic uncertainty causes an offset in emissions and does not impact year-to-year variability). Note that Fig. 4 shows the uncertainty due to the combined random and systematic error components.

To understand this reversal, we estimate global emissions of HCFC-141b using reported consumption data by adapting the approach taken by Simmonds et al. (2017), as detailed in Sect. 2.2.2. We estimate the prompt release fraction to be 24 (17–31) % and 37 (36–39) % of the annual consumption for Article 5 and non-Article 5 countries, respectively (68 % uncertainty interval). Our estimated annual bank release fraction is 3.6 (3.0–4.2) % from the remaining bank and 2.8 (1.9–3.9) % for Article 5 and non-Article 5 countries, respectively,

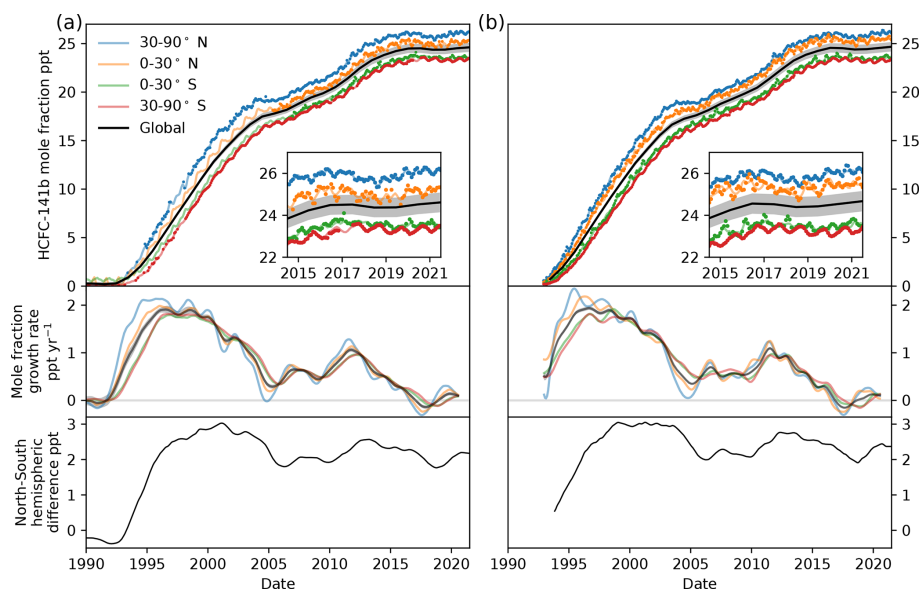


**Figure 3.** HCFC-141b global and semihemispheric mole fraction (top), growth rate (middle) and north–south interhemispheric difference (bottom) derived from AGAGE (a) and NOAA (b) measurements. Lines show mole fractions in each semihemisphere derived with the 12-box model using available data, whilst the dots represent the observations as monthly means of background measurements from all sites within each semihemisphere for each network. The grey shading shows the 1 standard deviation estimate in the global mean mole fraction. The north–south interhemispheric difference is a 12-month rolling mean.

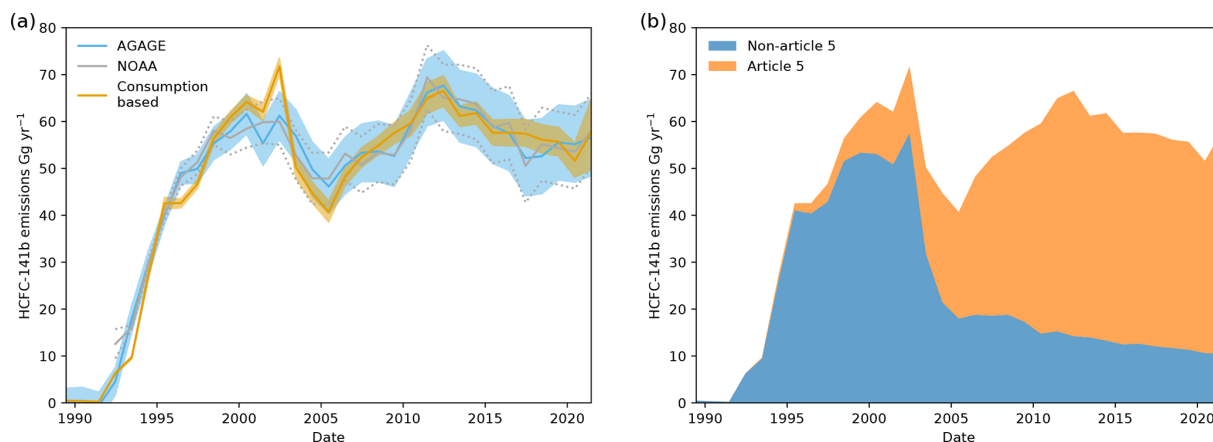


**Figure 4.** (a) HCFC-141b global emissions derived from AGAGE and NOAA measurements and derived from reported consumption data and estimated emission release fractions, where consumption has been predicted for 2021, assuming consumption in non-Article 5 countries is less than  $1 \text{ Gg yr}^{-1}$  and no constraints on Article 5 consumption. (b) A breakdown of HCFC-141b global emissions from Article 5 and non-Article 5 countries using the consumption-based emissions estimate, where 2021 consumption has been estimated from the top-down emissions data.

and is assumed to be unchanged since 1989. Simmonds et al. (2017) used an aggregated HCFC-141b prompt release fraction of  $34.5 \pm 4.0 \%$ , along with a bank release fraction of  $2.2 \%$ . Our estimated released fractions thus broadly agree with that used by Simmonds et al. (2017) and that previously estimated for closed foams containing CFC-11 (TEAP, 2019), which is  $25 \%$ – $35 \%$  for the prompt release fraction and  $1.5 \%$ – $4.2 \%$  for the bank release fraction. Using the reported consumption and estimated release fraction, we de-

rive the respective emissions using the top-down-informed bank model. Under the constraints of the top-down-informed bank model, we are able to estimate the necessary consumption needed to produce the observed top-down emissions in 2021, which has not yet been fully reported. This uses the reported consumption until 2020 and the estimated emissions rate from the bank to estimate the needed 2021 consumption to reproduce the top-down emissions estimate. This analysis, under the constraints of the model, suggests that consump-

tion likely rose between 2020 and 2021, from  $39 \text{ Gg yr}^{-1}$  in 2020 to  $67 (28\text{--}95) \text{ Gg yr}^{-1}$  in 2021. This consumption estimate for 2021 is very uncertain due to the uncertainty in the top-down-derived emissions, and so a decline in global emissions, and thus decline in consumption, cannot be excluded. Increasing consumption between 2017–2020 is not possible in this model, due the constraints imposed by the reported production and bank behaviour. An alternative conclusion that could be drawn from this analysis, under the assumption that reported consumption should decrease in 2021, is that the emissions rate from the bank has increased in more recent years, meaning that the inferred emissions rate, which is constant in time, is no longer representative and cannot adequately model emissions.

Figure 4a shows a comparison of the top-down atmospheric measurement-derived emissions, using the 12-box model (and without using information about reported consumption), and the emissions estimated using the top-down-informed bank model. Although these estimates are unique, they are not independent due to both top-down estimates using the same methodology to derive emissions using AGAGE and NOAA measurements and the dependence of the top-down-informed bank model on the estimates using AGAGE measurements. Figure 4b shows a breakdown of the mean emissions from non-Article 5 and Article 5 countries under the top-down-informed bank model using reported consumption data and assumptions inherent in the model, where 2021 consumption has been estimated. This imposes that all consumption in 2021 (over a maximum of  $1 \text{ Gg yr}^{-1}$ ) must come from Article 5 countries (see Sect. 2.2.2).

The timing of this increase in HCFC-141b emissions is nearly coincident with the rapid post-2018 global decline in CFC-11 emissions (Montzka et al., 2021), which may suggest that the enhanced apparent use and production of CFC-11 during 2012–2018, which was likely used for foam production, may have transitioned to HCFC-141b instead of transitioning to newer replacements. An explanation for the recent rise in global HCFC-141b emissions is, however, further complicated by a lack of understanding of the time-dependent changes in emissions from the existing HCFC-141b bank. Wang et al. (2015) suggest that HCFC-141b emissions in China are expected to peak in 2025–2027, 15 years after peak consumption in China. This is attributed to the release of HCFC-141b from foams during the disposal of insulated refrigerators and electric water heaters at their end of life around 15 years after peak consumption. If such a pattern predicted in China is applied to all developing countries, peak emissions from all developing countries would be expected around 2026–2027, 15 years after their peak consumption in 2011–2012, and could perhaps explain the observed emissions increase. However, a study in Lahore, Pakistan, showed that HCFC-141b emissions due to waste and disposal of HCFC-141b-containing refrigerators fell between 2005 and 2013 (Ul-Haq et al., 2016). It may therefore not be appropriate to extrapolate the bottom-up-predicted bank

emission trends in China to other developing countries, and there is likely considerable uncertainty and variation in the life cycle of appliances containing HCFC-141b foam and their disposal practices.

The top-down-informed bank model neglects emissions from feedstock and other so-called non-dispersive production. A typical emissions factor associated with fluorochemical production is around 4% (IPCC, 2019). If applied to global feedstock production, additional feedstock-related emissions would be  $0.5 \text{ Gg yr}^{-1}$  between 2017–2020, not enough to explain the global increase, with no increasing trend. Emissions factors from individual production facilities may vary considerably (0.1%–20%, 95% uncertainty, IPCC, 2019). A universal feedstock production leakage rate of 20% in 2020 compared to 0.1% in 2017 would be needed to explain the observed global increase in emissions. This would result in an additional  $3.0 \text{ Gg yr}^{-1}$  of emissions, compared to a mean global increase in the NOAA and AGAGE estimates of  $3.0 \pm 1.2 \text{ Gg yr}^{-1}$  during the same period. A sustained rapid deterioration in feedstock production losses since 2017 seems an unlikely scenario to explain the global increase in emissions.

In the following section we turn to regional emissions estimates of HCFC-141b, where observations are available, to further diagnose the driver behind the global rise.

### 3.2 East Asian emissions

Atmospheric measurement-based emissions estimates for east Asia are based on four different inverse methods using measurements from Gosan station, South Korea (see Sect. 2.1), and are combined into a single estimate using Monte Carlo sampling. These results provide emissions estimates for South Korea, North Korea and two regions that we denote eastern China (which includes the provinces of Anhui, Beijing, Hebei, Jiangsu, Liaoning, Shandong, Shanghai, Tianjin and Zhejiang) and western Japan (which includes the regions Chūgoku, Kansai, Kyūshū and Okinawa, and Shikoku), as measurements at Gosan have little sensitivity to emissions in western China or eastern Japan.

Emissions of HCFC-141b from eastern China show an increase in emissions from  $3.7 (1.8\text{--}4.8) \text{ Gg yr}^{-1}$  in 2008 to  $6.8 (3.7\text{--}9.4) \text{ Gg yr}^{-1}$  in 2020 and an increase of  $1.0 (-2.9, 3.8) \text{ Gg yr}^{-1}$  between 2017–2020. The 2017–2020 increase in eastern China could account for around a third of the global increase over the same period ( $3.0 \pm 1.2 \text{ Gg yr}^{-1}$ , NOAA and AGAGE mean), but given the large uncertainties this could explain all or none of the global increase. The mean emissions of the inverse frameworks (Fig. 5) generally agree well with bottom-up inventory estimates for China (Fang et al., 2018) scaled down to the eastern China region by population or gross domestic product from emissions from the whole of China (the range is shown by the orange shading in Fig. 5), given the uncertainties in the top-down modelling and the uncertainties likely present in the bottom-up model

(which were not given in the study). The top-down-derived emissions trend is also supported by the projected emissions of Wang et al. (2015), although emissions projected by Wan et al. (2009) were expected to peak in 2018. If the bottom-up-predicted emissions by Wang et al. (2015) and Fang et al. (2018) come to fruition, HCFC-141b emissions from China will continue to rise until the mid-2020s. Our results presented here for eastern China contrast with top-down estimates presented for the whole of China in previous studies (Fang et al., 2019b; Yi et al., 2021), which suggest a continual fall in emissions.

Emissions from South Korea (around  $1\text{--}3\text{ Gg yr}^{-1}$ ) are smaller than from eastern China, and it is uncertain whether they are increasing or decreasing. Emissions from western Japan and North Korea are even smaller (generally less than around  $1\text{ Gg yr}^{-1}$ ). Japan, in contrast to other east Asian countries, legislates the removal and destruction of HCFC refrigerants and HCFCs in foams within appliances through the Home Appliance Recycling Act (Hotta et al., 2016).

### 3.3 Northwestern European emissions

Emissions for northwestern Europe (Belgium, France, Germany, Ireland, Luxembourg, the Netherlands and the United Kingdom) were estimated using the InTEM inversion system, based on measurements from Mace Head in Ireland, starting in 1994, with additional measurements from Jungfraujoch in Switzerland from 2008, Monte Cimone in Italy from 2012, Tacolneston in the UK from 2012 and Taunus in Germany from 2013. NW Europe sees a sharp fall in emissions after 2003, Fig. 6a, from  $3.6 \pm 0.9$  in 2003 to  $2.2 \pm 1.0\text{ Gg yr}^{-1}$  in 2004 and then  $1.3 \pm 0.9\text{ Gg yr}^{-1}$  in 2005, with timing consistent with the phase-down of HCFC production in those countries. Emissions have steadily fallen since, reaching  $0.4 \pm 0.1\text{ Gg yr}^{-1}$  in 2020. Emissions from individual countries are presented in the Supplement.

Emissions in NW Europe peak coincidentally with high consumption in developed countries. The European Union's Regulation (EC) 1005/2009 (and similar legislation in the UK) requires that appliance foam insulation controlled under the Montreal Protocol is recovered at disposal to be recycled or properly destroyed. Therefore we expect relatively low end-of-life emissions in NW Europe, in comparison to the emissions rates in China, and our results provide evidence that such legislation has, likely, been effective.

### 3.4 Contiguous US emissions

Top-down emissions estimates for the contiguous United States from 2015 to 2020 (Fig. 6a) are derived from measurements made by NOAA's North American sampling network (see Sect. 2.3.5 and 2.1) using two atmospheric transport models and the NOAA inversion framework (Sect. 2.3.5, Hu et al., 2016). Taking an average of the two top-down estimates for the United States, emissions likely increased

slightly between 2015 and 2017, with  $5.5 \pm 0.6$  in 2015 and  $6.4 \pm 0.7\text{ Gg yr}^{-1}$  in 2017. The HYSPLIT-NAM model estimate suggests that emissions remain unchanged in 2018 at  $6.3 \pm 0.6$  and fall to  $5.3 \pm 1.0\text{ Gg yr}^{-1}$  in 2020. Bottom-up emissions estimates by the U.S. Environmental Protection Agency (EPA, 2021) over the same period (Fig. 6a) suggest that emissions fell from 8.6 in 2015 to  $7.1\text{ Gg yr}^{-1}$  in 2017 to  $6.7\text{ Gg yr}^{-1}$  in 2020. The reason for the discrepancy in the trend between the top-down and bottom-up estimates in 2015–2016 is unclear; however both show only small changes in emissions between 2017–2020. The NOAA top-down estimates are 10%–40% smaller than the U.S. EPA bottom-up estimates (assuming that the non-contiguous states and territories are not responsible for the discrepancy).

Consumption of HCFCs in the United States from 2002 to 2003 fell to around half and has continued to decline. The U.S. EPA emission estimate suggests peak emissions many years after a peak consumption, different from what the NW European top-down emissions show and more similar to bottom-up projections for China. The reason for a slowing in the decline of emissions since 2017 is not fully clear, but the bottom-up model suggests that it may be due to post-disposal emissions from polyurethane foams used for domestic refrigerator and freezer insulation, occurring during the 26 years following disposal (EPA, 2021). This assumes that domestic refrigerators and freezers have a lifetime of 14 years and that the leakage post-disposal (2%) is higher than that during the appliance lifetime (0.25%). In the United States, a gradual increase in HCFC-141b emissions due to the disposal of domestic refrigerants following a peak in consumption may be occurring, much like that predicted to occur in China, offsetting reductions in other banks. Unlike the European Union, which mandates destruction of HCFC-141b within refrigerator foams, the U.S. EPA's Responsible Appliance Disposal (RAD) Program is voluntary. This may explain different US and European HCFC-141b emission patterns, despite similar consumption patterns.

### 3.5 Australian emissions

Top-down HCFC-141b emissions estimates using InTEM show that emissions in Australia have remained largely constant from 2000 to 2021, perhaps showing a slight decline (Fig. 6b).

Australia has not produced or exported HCFC-141b, and therefore HCFC-141b consumption is governed by imports, assuming that no significant stockpiling for later use occurred. Australian HCFC-141b imports/consumption commenced in the early 1990s, reaching 0.8–0.9 Gg in 1999 and then declining to zero by 2012, well ahead of the mandated HCFC phase-out schedule (Dunse et al., 2021). From 1991 to 2012, Australian HCFC-141b imports totalled 7.8 Gg.

Assuming that emissions have therefore only come from the bank, and using the emissions factor derived for non-Article 5 countries from Sect. 3.1, we derive a bottom-up

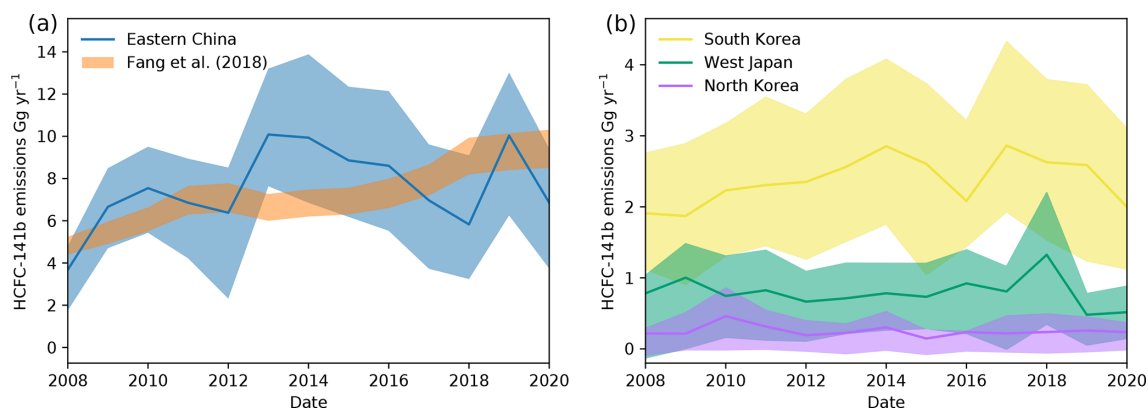


**Figure 5.** Emissions estimates for east Asia. **(a)** Combined top-down emissions from four inversion frameworks for eastern China with their 68 % uncertainties (blue). Bottom-up emissions estimates for eastern China (orange) estimated by scaling down the Fang et al. (2018) estimate for the whole of China by either population or gross domestic product to eastern China. The shading shows the range between these two metrics for scaling. **(b)** Top-down estimates for South Korea, western Japan and North Korea.

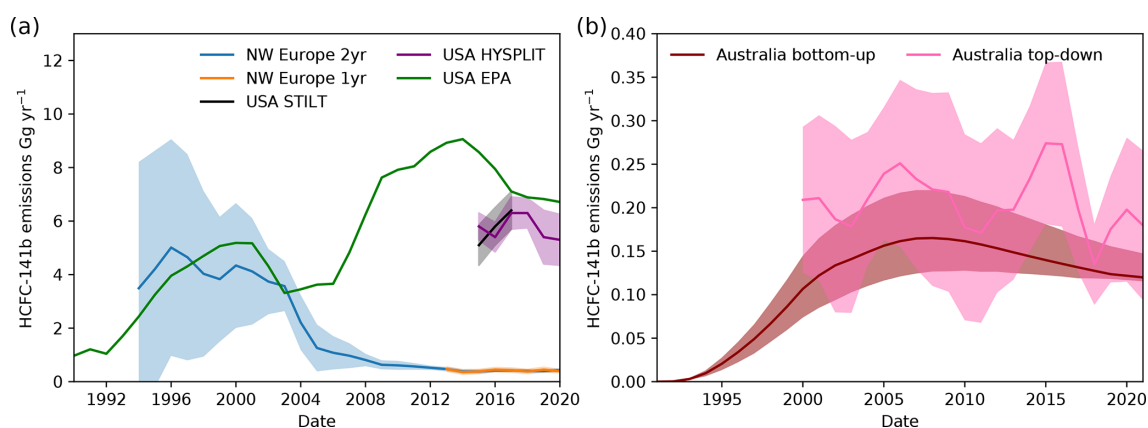


**Figure 6.** **(a)** Annual InTEM emissions from northwestern Europe using a 2-year inversion period (blue) or only a single year (orange) and from the contiguous United States using two transport models, HYSPLIT (purple, 2015–2020) and STILT (black, 2015–2017). Bottom-up estimates for the United States are shown in green. **(b)** Annual InTEM emissions for Australia (pink) and bottom-up emissions estimated using consumption data (dark red).

emissions estimate based on consumption in Australia. The bottom-up model likely underestimates the emissions release rate because prompt emissions, which we assume to include emissions during installation and immediate usage, have not been included. The top-down and bottom-up estimates for Australia generally agree, given the large uncertainties. Australia has no laws to mandate the destruction of HCFCs within appliance-insulating foams at disposal. However, there is no obvious increase in HCFC-141b emissions in Australia in recent years due to an increase in the rate of emissions from foam-containing appliances when they reach their end of life (within uncertainties).

#### 4 Conclusions

For 5 years after the reported 2012 peak in HCFC-141b production, global emissions of the ozone-depleting substance

HCFC-141b declined. However, the trend reversed and emissions increased by  $3.0 \pm 1.2 \text{ Gg yr}^{-1}$  or 6 % from 2017 to 2021, even though reported production for dispersive uses continued to decrease. This timing is similar to a decline in global emissions of CFC-11, the ozone-depleting substance replaced by HCFC-141b for foam blowing, following a period of increasing global CFC-11 emissions, of which  $60 \pm 40\%$  could be attributed to eastern China (Park et al., 2021). Due to a current incomplete understanding of the size and behaviour of the global HCFC-141b bank, it is uncertain whether the emission rise is due to unreported production for dispersive uses, as suggested by a simple bottom-up model constrained by measurement-derived emissions; due to emissions at the end of life of foam-containing products; or due to a combination thereof.

An increase due to emissions from the bank is suggested by bottom-up emissions projections for China due to the dis-

posal of appliances containing HCFC-141b foam, without destroying the HCFC-141b. However, according to bottom-up and top-down estimates, emissions from China alone cannot fully explain the global rise. This pattern of bank-related emissions years after peak consumption may not apply to other developing countries. Emissions in the United States and Australia, where there are no strict requirements in place for the destruction of HCFCs upon appliance disposal, do not show evidence of declining, or increasing, emissions in recent years. This contrasts with the European Union, which mandates more complete HCFC destruction upon disposal, where emissions have decreased continuously since the phase-out of consumption began. A lack of declining emissions in the United States and Australia may support the argument that a change in emissions rates from the foam banks after the disposal of foam-containing appliances is driving the rise in emissions.

Emissions of HCFC-141b feedstock is unlikely to be the cause of the global increase, unless emission rates during production have rapidly increased, from near-zero losses to around a fifth of production. The amount and fate of HCFC-141b produced as a byproduct are unknown, and we have no evidence to suggest that this pathway leads to significant emissions or would have changed substantially since 2017 in a way that could explain the global emission increase.

The regional-scale emissions considered here only account for around 30 % of global emissions in 2020. The combined regional-scale emissions decreased by  $2.3 \pm 4.6 \text{ Gg yr}^{-1}$  between 2017–2020, compared to a mean global increase in the NOAA and AGAGE estimates of  $3.0 \pm 1.2 \text{ Gg yr}^{-1}$  during the same period. It seems likely that a substantial recent increase in emissions is coming from regions that we have not studied here.

We cannot demonstrate a conclusive driver behind the 2017–2021 increase in global emissions, given the information available. A better understanding of the behaviour of the HCFC-141b bank and its expected emissions, and more widespread measurement-based emissions monitoring, would aid in understanding the causes for the current rise in HCFC-141b emissions.

**Code and data availability.** AGAGE data are available at <http://agage.mit.edu/data/agage-data> (last access: 17 March 2022) and <https://doi.org/10.15485/1841748> (Prinn et al., 2022). NOAA atmospheric observations are available at the NOAA atmospheric observations are available at the NOAA/GML website (updated from Montzka et al., 2015; <https://gml.noaa.gov/hats/>, last access: 6 April 2022). Measurements of archived air samples are available in the Supplement. The 12-box model and the inverse method used to quantify emissions are available via GitHub, <https://github.com/mrghg/py12box> (last access: 20 July 2022), [https://github.com/mrghg/py12box\\_invert](https://github.com/mrghg/py12box_invert) (last access: 20 July 2022), and Zenodo (<https://doi.org/10.5281/zenodo.6857447>, Rigby and Western, 2022a, <https://doi.org/10.5281/zenodo.685779>, Rigby and Western, 2022b). Inputs to this model are avail-

able in the Supplement. The NAME model and InTEM models are available for research purposed via request to the UK Met Office ([enquiries@metoffice.gov.uk](mailto:enquiries@metoffice.gov.uk)) or on request to Alistair J. Manning or Alison L. Redington. The FLEXPART model is available from <https://www.flexpart.eu> (Pisso et al., 2019). The EBRIS algorithm is available from <https://doi.org/10.5281/zenodo.1194642> (Henne, 2018). The Bristol MCMC inversion code is available at <https://github.com/ACRG-Bristol/acrg> (last access: 20 July 2022) (<https://doi.org/10.5281/zenodo.6834888>, Rigby et al., 2022). The code for the FLEXPART-MIT inversion is available from Xuekun Fang upon request. The code for the NOAA inversion is available from Lei Hu upon request.

**Supplement.** The supplement related to this article is available online at: <https://doi.org/10.5194/acp-22-9601-2022-supplement>.

**Author contributions.** LMW led the writing of the manuscript with contributions from ALR, AJM, CMT, LH, SH, JM, SR, MKV, SAM, MR, and all other coauthors. LWM, ALR, AJM, CMT, LH, SH and XF performed inverse modelling. LJMK provided data on reported consumption and production. DSG provided bottom-up US HCFC-141b emissions. LJMK, CT and DSG provided input on HCFC-141b uses, the behaviour of the banks and appliance life cycles. BD provided data and analysis on Australian consumption and emissions. JM assisted with data curation. JA, AE, PJF, CMH, PBK, MM, SAM, JM, SO'D, HP, SP, SR, PKS, DS, RS, TS, CS, KMS, IV, MKV and DY provided measurement data. SAM, RGP, MR and RFW provided oversight to the work and the measurement networks.

**Competing interests.** The contact author has declared that none of the authors has any competing interests.

**Disclaimer.** Publisher's note: Copernicus Publications remains neutral with regard to jurisdictional claims in published maps and institutional affiliations.

**Special issue statement.** This article is part of the special issue "Atmospheric ozone and related species in the early 2020s: latest results and trends (ACP/AMT inter-journal SI)". It is a result of the 2021 Quadrennial Ozone Symposium (QOS) held online on 3–9 October 2021.

**Acknowledgements.** We thank the site operators for their continued support to maintain the measurements at the AGAGE and NOAA stations and the NOAA and CIRES personnel for technical and logistical support of facilitating the collection of tower and aircraft samples throughout North America. We thank Arlyn Andrews for providing the WRF-STILT footprints and Nada Derek for Cape Grim data analysis. We greatly thank Phil DeCola for supporting some of NOAA's inverse modelling analyses. The NASA Upper Atmosphere Research Program supports AGAGE (in-

cluding partial support of Mace Head, Ragged Point and Cape Grim and full support of Trinidad Head and Cape Matatula through grant NNX16AC98G to MIT and grants NNX16AC96G and NNX16AC97G to SIO and multiple preceding grants. Mace Head and Tacolneston station and InTEM are supported by the UK Department of Business, Energy and Industrial Strategy (BEIS contract 1537/06/2018). Cape Grim station is supported by the Australian Bureau of Meteorology, CSIRO, the Australian Department of Agriculture, Water and the Environment (DAWE), and Refrigerant Reclaim Australia (RRA). Funding for NOAA measurements was provided in part by the NOAA Climate Program Office's Atmospheric Chemistry, Carbon Cycle, and Climate (AC4) Program and by the NOAA Cooperative Agreement with CIRES, NA17OAR4320101. NOAA's HYSPLIT-NAMS footprints simulations were supported by NOAA Climate Program Office's AC4 programme and Climate Observations and Monitoring (COM) programme, grant number NA21OAR4310233. NOAA's inverse modelling analysis was partially supported by the Grantham foundation and GIST.earth LLC. Computation at the University of Bristol was carried out by the University of Bristol BluePebble high-performance computing facility. FLEXPART simulations were carried out at the Swiss National Supercomputing Centre (CSCS) under project ID s862. Luke M. Western received funding from the European Union's Horizon 2020 research and innovation programme under Marie Skłodowska-Curie grant agreement no. 101030750. Luke M. Western and Matthew Rigby were also supported by Natural Environment Research Council (NERC) grants NE/N016548/1 and R100529-101. Alistair J. Manning and Alison L. Redington are supported by the Met Office Hadley Centre Climate Programme, funded by the UK's Department for Business, Energy and Industrial Strategy and Department for Environment, Food and Rural Affairs. Sunyoung Park and Hyeri Park are supported by the National Research Foundation of Korea (NRF) grant funded by the South Korean government (MSIT) (no. 2020R1A2C3003774). Lambert J. M. Kuijpers is supported by the Ozone Secretariat in Nairobi, which is partly funded for supporting this work by grants from the European Commission, Brussels.

**Financial support.** This research has been supported by the H2020 Marie Skłodowska-Curie Actions (grant no. 101030750); the National Aeronautics and Space Administration (grant nos. NNX16AC98G, NNX16AC96G, and NNX16AC97G); the Department for Business, Energy and Industrial Strategy, UK Government (grant no. 1537/06/2018); the Climate Program Office (grant no. NA21OAR4310233); the Natural Environment Research Council (grant nos. NE/N016548/1 and R100529-101); and the National Research Foundation of Korea (grant no. 2020R1A2C3003774).

**Review statement.** This paper was edited by Gabriele Stiller and reviewed by two anonymous referees.

## References

Andersen, S. O., Gao, S., Carvalho, S., Ferris, T., Gonzalez, M., Sherman, N. J., Wei, Y., and Zaelke, D.: Narrowing feedstock exemptions under the Montreal Protocol has multiple environ-

mental benefits, *P. Natl. Acad. Sci. USA*, 118, e2022668118, <https://doi.org/10.1073/pnas.2022668118>, 2021.

Arnold, T., Mühle, J., Salameh, P. K., Harth, C. M., Ivy, D. J., and Weiss, R. F.: Automated Measurement of Nitrogen Trifluoride in Ambient Air, *Anal. Chem.*, 84, 4798–4804, <https://doi.org/10.1021/ac300373e>, 2012.

Burkholder, J. B.: Appendix A: Summary of Abundances, Lifetimes, ODPs, REs, GWPs, and GTPs, in: *Scientific Assessment of Ozone Depletion: 2018*, vol. 58, Global Ozone Research and Monitoring Project, World Meteorological Organization, Geneva, Switzerland, [https://csl.noaa.gov/assessments/ozone/2018/downloads/AppendixA\\_2018OzoneAssessment.pdf](https://csl.noaa.gov/assessments/ozone/2018/downloads/AppendixA_2018OzoneAssessment.pdf) (last access: 14 July 2022), 2019.

Cunnold, D. M., Prinn, R. G., Rasmussen, R. A., Simmonds, P. G., Alyea, F. N., Cardelino, C. A., Crawford, A. J., Fraser, P. J., and Rosen, R. D.: The Atmospheric Lifetime Experiment: 3. Lifetime methodology and application to three years of CFC13 data, *J. Geophys. Res.-Oceans*, 88, 8379–8400, <https://doi.org/10.1029/JC088iC13p08379>, 1983.

Dunse, B., Derek, N., Fraser, P., and Krummel, P.: Australian and Global Emissions of Ozone Depleting Substances, Report prepared for the Australian Government Department of Agriculture, Water and the Environment, Tech. Rep., CSIRO Oceans and Atmosphere, Melbourne, Australia, iii, 57 pp., <https://www.agriculture.gov.au/sites/default/files/documents/australian-global-emissions-ozone-depleting-substances.pdf> (last access: 14 July 2022), 2021.

Engel, A. and Rigby, M.: Chapter 1: Update on Ozone Depleting Substances (ODSs) and Other Gases of Interest to the Montreal Protocol, in: *Scientific Assessment of Ozone Depletion: 2018*, vol. 58, Global Ozone Research and Monitoring Project, World Meteorological Organization, Geneva, Switzerland, [https://csl.noaa.gov/assessments/ozone/2018/downloads/Chapter1\\_2018OzoneAssessment.pdf](https://csl.noaa.gov/assessments/ozone/2018/downloads/Chapter1_2018OzoneAssessment.pdf) (last access: 14 July 2022), 2019.

EPA: Inventory of U.S. Greenhouse Gas Emissions and Sinks: 1990–2019, Tech. rep., The United States Environmental Protection Agency (EPA), <https://www.epa.gov/ghgemissions/inventory-us-greenhouse-gas-emissions-and-sinks> (last access: 14 July 2022), 2021.

Fang, X., Ravishankara, A. R., Velders, G. J. M., Molina, M. J., Su, S., Zhang, J., Hu, J., and Prinn, R. G.: Changes in Emissions of Ozone-Depleting Substances from China Due to Implementation of the Montreal Protocol, *Environ. Sci. Technol.*, 52, 11359–11366, <https://doi.org/10.1021/acs.est.8b01280>, 2018.

Fang, X., Park, S., Saito, T., Tunnicliffe, R., Ganesan, A. L., Rigby, M., Li, S., Yokouchi, Y., Fraser, P. J., Harth, C. M., Krummel, P. B., Mühle, J., O'Doherty, S., Salameh, P. K., Simmonds, P. G., Weiss, R. F., Young, D., Lunt, M. F., Manning, A. J., Gressent, A., and Prinn, R. G.: Rapid increase in ozone-depleting chloroform emissions from China, *Nat. Geosci.*, 12, 89–93, <https://doi.org/10.1038/s41561-018-0278-2>, 2019a.

Fang, X., Yao, B., Vollmer, M. K., Reimann, S., Liu, L., Chen, L., Prinn, R. G., and Hu, J.: Changes in HCFC Emissions in China During 2011–2017, *Geophys. Res. Lett.*, 46, 10034–10042, <https://doi.org/10.1029/2019GL083169>, 2019b.

Fraser, P. J., Pearman, G. I., and Derek, N.: CSIRO Non-carbon Dioxide Greenhouse Gas Research. Part 1: 1975–90, *Hist. Rec. Aust. Sci.*, 29, 1–13, <https://doi.org/10.1071/HR17016>, 2018.

- Ganesan, A. L., Rigby, M., Zammit-Mangion, A., Manning, A. J., Prinn, R. G., Fraser, P. J., Harth, C. M., Kim, K.-R., Krummel, P. B., Li, S., Mühle, J., O'Doherty, S. J., Park, S., Salameh, P. K., Steele, L. P., and Weiss, R. F.: Characterization of uncertainties in atmospheric trace gas inversions using hierarchical Bayesian methods, *Atmos. Chem. Phys.*, 14, 3855–3864, <https://doi.org/10.5194/acp-14-3855-2014>, 2014.
- Gelman, A. and Rubin, D. B.: Inference from Iterative Simulation Using Multiple Sequences, *Stat. Sci.*, 7, 457–472, <https://doi.org/10.1214/ss/1177011136>, 1992.
- Henne, S.: R Packages For Atmospheric Emission Inversion, Zenodo [code], <https://doi.org/10.5281/zenodo.1194642>, 2018.
- Henne, S., Brunner, D., Oney, B., Leuenberger, M., Eugster, W., Bamberger, I., Meinhardt, F., Steinbacher, M., and Emmenegger, L.: Validation of the Swiss methane emission inventory by atmospheric observations and inverse modelling, *Atmos. Chem. Phys.*, 16, 3683–3710, <https://doi.org/10.5194/acp-16-3683-2016>, 2016.
- Hotta, Y., Santo, A., and Tasaki, T.: Recycling of electronic home appliances in Japan, in: *Extended Producer Responsibility: Updated Guidance for Efficient Waste Management*, OECD Publishing, Paris, 263–238, <https://doi.org/10.1787/9789264256385-17-en>, 2016.
- Hu, L., Montzka, S. A., Miller, J. B., Andrews, A. E., Lehman, S. J., Miller, B. R., Thoning, K., Sweeney, C., Chen, H., Godwin, D. S., Masarie, K., Bruhwiler, L., Fischer, M. L., Biraud, S. C., Torn, M. S., Mountain, M., Nehr Korn, T., Eluszkiewicz, J., Miller, S., Draxler, R. R., Stein, A. F., Hall, B. D., Elkins, J. W., and Tans, P. P.: U.S. emissions of HFC-134a derived for 2008–2012 from an extensive flask-air sampling network, *J. Geophys. Res.-Atmos.*, 120, 801–825, <https://doi.org/10.1002/2014JD022617>, 2015.
- Hu, L., Montzka, S. A., Miller, B. R., Andrews, A. E., Miller, J. B., Lehman, S. J., Sweeney, C., Miller, S. M., Thoning, K., Siso, C., Atlas, E. L., Blake, D. R., de Gouw, J., Gilman, J. B., Dutton, G., Elkins, J. W., Hall, B., Chen, H., Fischer, M. L., Mountain, M. E., Nehr Korn, T., Biraud, S. C., Moore, F. L., and Tans, P.: Continued emissions of carbon tetrachloride from the United States nearly two decades after its phaseout for dispersive uses, *P. Natl. Acad. Sci. USA*, 113, 2880–2885, <https://doi.org/10.1073/pnas.1522284113>, 2016.
- Hu, L., Montzka, S. A., Lehman, S. J., Godwin, D. S., Miller, B. R., Andrews, A. E., Thoning, K., Miller, J. B., Sweeney, C., Siso, C., Elkins, J. W., Hall, B. D., Mondeel, D. J., Nance, D., Nehr Korn, T., Mountain, M., Fischer, M. L., Biraud, S. C., Chen, H., and Tans, P. P.: Considerable contribution of the Montreal Protocol to declining greenhouse gas emissions from the United States, *Geophys. Res. Lett.*, 44, 8075–8083, <https://doi.org/10.1002/2017GL074388>, 2017.
- Hu, L., Montzka, S. A., Kaushik, A., Andrews, A. E., Sweeney, C., Miller, J., Baker, I. T., Denning, S., Campbell, E., Shiga, Y. P., Tans, P., Siso, M. C., Crotwell, M., McKain, K., Thoning, K., Hall, B., Vimont, I., Elkins, J. W., Whelan, M. E., and Suntharalingam, P.: COS-derived GPP relationships with temperature and light help explain high-latitude atmospheric CO<sub>2</sub> seasonal cycle amplification, *P. Natl. Acad. Sci. USA*, 118, e2103423118, <https://doi.org/10.1073/pnas.2103423118>, 2021.
- IPCC: Chemical Industry Emissions, in: *2019 Refinement to the 2006 IPCC Guidelines for National Greenhouse Gas Inventories*, edited by: Calvo Buendia, E., Tanabe, K., Kranjc, A., Baasansuren, J., Fukuda, M., Ngarize, S., Osako, A., Pyrozhenko, Y., Shermanau, P., and Federici, S., vol. 3, chap. 3, IPCC, Switzerland, [https://www.ipcc-nggip.iges.or.jp/public/2019rf/pdf/3\\_Volume3/19R\\_V3\\_Ch03\\_Chemical\\_Industry.pdf](https://www.ipcc-nggip.iges.or.jp/public/2019rf/pdf/3_Volume3/19R_V3_Ch03_Chemical_Industry.pdf) (last access: 14 July 2022), 2019.
- Janssens-Maenhout, G., Crippa, M., Guizzardi, D., Muntean, M., and Schaaf, E.: Emissions Database for Global Atmospheric Research, version v4.2 (time-series), Joint Research Centre Data Catalogue [data set], <http://data.europa.eu/89h/jrc-edgar-emissiontimeseriesv42>, 2011.
- Jones, A., Thomson, D., Hort, M., and Devenish, B.: The U.K. Met Office's Next-Generation Atmospheric Dispersion Model, NAME III, in: *Air Pollution Modeling and Its Application XVII*, Springer US, Boston, MA, 580–589, [https://doi.org/10.1007/978-0-387-68854-1\\_62](https://doi.org/10.1007/978-0-387-68854-1_62), ISBN 978-0-387-68854-1, 2007.
- Keller, C. A., Hill, M., Vollmer, M. K., Henne, S., Brunner, D., Reimann, S., O'Doherty, S., Arduini, J., Maione, M., Ferenczi, Z., Haszpra, L., Manning, A. J., and Peter, T.: European Emissions of Halogenated Greenhouse Gases Inferred from Atmospheric Measurements, *Environ. Sci. Technol.*, 46, 217–225, <https://doi.org/10.1021/es202453j>, 2012.
- Maione, M., Giostra, U., Arduini, J., Furlani, F., Graziosi, F., Lo Vullo, E., and Bonasoni, P.: Ten years of continuous observations of stratospheric ozone depleting gases at Monte Cimone (Italy) – Comments on the effectiveness of the Montreal Protocol from a regional perspective, *Sci. Total Environ.*, 445–446, 155–164, <https://doi.org/10.1016/j.scitotenv.2012.12.056>, 2013.
- Manning, A. J., Redington, A. L., Say, D., O'Doherty, S., Young, D., Simmonds, P. G., Vollmer, M. K., Mühle, J., Arduini, J., Spain, G., Wisher, A., Maione, M., Schuck, T. J., Stanley, K., Reimann, S., Engel, A., Krummel, P. B., Fraser, P. J., Harth, C. M., Salameh, P. K., Weiss, R. F., Gluckman, R., Brown, P. N., Watterson, J. D., and Arnold, T.: Evidence of a recent decline in UK emissions of hydrofluorocarbons determined by the InTEM inverse model and atmospheric measurements, *Atmos. Chem. Phys.*, 21, 12739–12755, <https://doi.org/10.5194/acp-21-12739-2021>, 2021.
- MCTOC: Medical and Chemicals Technical Options Committee: 2018 Assessment Report, 1, United Nations Environment Programme, ISBN 978-9966-076-51-9, <https://ozone.unep.org/sites/default/files/2019-04/MCTOC-Assessment-Report-2018.pdf> (last access: 14 July 2022), 2018.
- Michalak, A. M., Hirsch, A., Bruhwiler, L., Gurney, K. R., Peters, W., and Tans, P. P.: Maximum likelihood estimation of covariance parameters for Bayesian atmospheric trace gas surface flux inversions, *J. Geophys. Res.-Atmos.*, 110, D24107, <https://doi.org/10.1029/2005JD005970>, 2005.
- Miller, B. R., Weiss, R. F., Salameh, P. K., Tanhua, T., Grealley, B. R., Mühle, J., and Simmonds, P. G.: Medusa : A Sample Preconcentration and GC/MS Detector System for in Situ Measurements of Atmospheric Trace Halocarbons, Hydrocarbons, and Sulfur Compounds, *Anal. Chem.*, 80, 1536–1545, <https://doi.org/10.1021/ac702084k>, 2008.
- Montzka, S. A., McFarland, M., Andersen, S. O., Miller, B. R., Fahey, D. W., Hall, B. D., Hu, L., Siso, C., and Elkins, J. W.: Recent Trends in Global Emissions of Hydrochlorofluorocarbons and Hydrofluorocarbons: Reflecting on the 2007 Adjustments

- to the Montreal Protocol, *J. Phys. Chem. A*, 119, 4439–4449, <https://doi.org/10.1021/jp5097376>, 2015.
- Montzka, S. A., Dutton, G. S., Yu, P., Ray, E., Portmann, R. W., Daniel, J. S., Kuijpers, L., Hall, B. D., Mondeel, D., Siso, C., Nance, J. D., Rigby, M., Manning, A. J., Hu, L., Moore, F., Miller, B. R., and Elkins, J. W.: An unexpected and persistent increase in global emissions of ozone-depleting CFC-11, *Nature*, 557, 413–417, <https://doi.org/10.1038/s41586-018-0106-2>, 2018.
- Montzka, S. A., Dutton, G. S., Portmann, R. W., Chipperfield, M. P., Davis, S., Feng, W., Manning, A. J., Ray, E., Rigby, M., Hall, B. D., Siso, C., Nance, J. D., Krummel, P. B., Mühle, J., Young, D., O'Doherty, S., Salameh, P. K., Harth, C. M., Prinn, R. G., Weiss, R. F., Elkins, J. W., Walter-Terrinoni, H., and Theodoridi, C.: A decline in global CFC-11 emissions during 2018–2019, *Nature*, 590, 428–432, <https://doi.org/10.1038/s41586-021-03260-5>, 2021.
- Mühle, J., Ganesan, A. L., Miller, B. R., Salameh, P. K., Harth, C. M., Grealley, B. R., Rigby, M., Porter, L. W., Steele, L. P., Trudinger, C. M., Krummel, P. B., O'Doherty, S., Fraser, P. J., Simmonds, P. G., Prinn, R. G., and Weiss, R. F.: Perfluorocarbons in the global atmosphere: tetrafluoromethane, hexafluoroethane, and octafluoropropane, *Atmos. Chem. Phys.*, 10, 5145–5164, <https://doi.org/10.5194/acp-10-5145-2010>, 2010.
- Mühle, J., Trudinger, C. M., Western, L. M., Rigby, M., Vollmer, M. K., Park, S., Manning, A. J., Say, D., Ganesan, A., Steele, L. P., Ivy, D. J., Arnold, T., Li, S., Stohl, A., Harth, C. M., Salameh, P. K., McCulloch, A., O'Doherty, S., Park, M.-K., Jo, C. O., Young, D., Stanley, K. M., Krummel, P. B., Mitrevski, B., Hermansen, O., Lunder, C., Evangelidou, N., Yao, B., Kim, J., Hmiel, B., Buizert, C., Petrenko, V. V., Arduini, J., Maione, M., Etheridge, D. M., Michalopoulou, E., Czerniak, M., Severinghaus, J. P., Reimann, S., Simmonds, P. G., Fraser, P. J., Prinn, R. G., and Weiss, R. F.: Perfluorocyclobutane (PFC-318, *c*-C<sub>4</sub>F<sub>8</sub>) in the global atmosphere, *Atmos. Chem. Phys.*, 19, 10335–10359, <https://doi.org/10.5194/acp-19-10335-2019>, 2019.
- Multilateral Fund: UNEP/OzL.Pro/ExCom/84/9/Rev.1 Country Programme Data and Prospects for Compliance, Tech. Rep., Executive Committee of The Multilateral Fund for the Implementation of the Montreal Protocol, <http://www.multilateralfund.org/84/English/1/8409r1p1.pdf> (last access: 14 July 2022), 2019.
- O'Doherty, S., Simmonds, P. G., Cunnold, D. M., Wang, H. J., Sturrock, G. A., Fraser, P. J., Ryall, D., Derwent, R. G., Weiss, R. F., Salameh, P., Miller, B. R., and Prinn, R. G.: In situ chloroform measurements at Advanced Global Atmospheric Gases Experiment atmospheric research stations from 1994 to 1998, *J. Geophys. Res.-Atmos.*, 106, 20429–20444, <https://doi.org/10.1029/2000JD900792>, 2001.
- Park, S., Western, L. M., Saito, T., Redington, A. L., Henne, S., Fang, X., Prinn, R. G., Manning, A. J., Montzka, S. A., Fraser, P. J., Ganesan, A. L., Harth, C. M., Kim, J., Krummel, P. B., Liang, Q., Mühle, J., O'Doherty, S., Park, H., Park, M.-K., Reimann, S., Salameh, P. K., Weiss, R. F., and Rigby, M.: A decline in emissions of CFC-11 and related chemicals from eastern China, *Nature*, 590, 433–437, <https://doi.org/10.1038/s41586-021-03277-w>, 2021.
- Pisso, I., Sollum, E., Grythe, H., Kristiansen, N. I., Casiani, M., Eckhardt, S., Arnold, D., Morton, D., Thompson, R. L., Groot Zwaaftink, C. D., Evangelidou, N., Sode-  
mann, H., Haimberger, L., Henne, S., Brunner, D., Burkhardt, J. F., Fouilloux, A., Brioude, J., Philipp, A., Seibert, P., and Stohl, A.: The Lagrangian particle dispersion model FLEX-PART version 10.4, *Geosci. Model Dev.*, 12, 4955–4997, <https://doi.org/10.5194/gmd-12-4955-2019>, 2019.
- Prinn, R., Weiss, R., Arduini, J., Arnold, T., DeWitt, H. L., Fraser, P., Ganesan, A., Gasore, J., Harth, C., Hermansen, O., Kim, J., Krummel, P., Loh, Z., Lunder, C., Maione, M., Manning, A., Miller, B., Mitrevski, B., Mühle, J., O'Doherty, S., Park, S., Reimann, S., Rigby, M., Saito, T., Salameh, P., Schmidt, R., Simmonds, P., Steele, P., Vollmer, M., Hsiang-Jui (Ray), W., Yao, B., Young, D., and Zhou, L.: The Advanced Global Atmospheric Gases Experiment (AGAGE) Data, ESS-DIVE repository [data set], <https://doi.org/10.15485/1841748>, 2022.
- Prinn, R. G., Weiss, R. F., Arduini, J., Arnold, T., DeWitt, H. L., Fraser, P. J., Ganesan, A. L., Gasore, J., Harth, C. M., Hermansen, O., Kim, J., Krummel, P. B., Li, S., Loh, Z. M., Lunder, C. R., Maione, M., Manning, A. J., Miller, B. R., Mitrevski, B., Mühle, J., O'Doherty, S., Park, S., Reimann, S., Rigby, M., Saito, T., Salameh, P. K., Schmidt, R., Simmonds, P. G., Steele, L. P., Vollmer, M. K., Wang, R. H., Yao, B., Yokouchi, Y., Young, D., and Zhou, L.: History of chemically and radiatively important atmospheric gases from the Advanced Global Atmospheric Gases Experiment (AGAGE), *Earth Syst. Sci. Data*, 10, 985–1018, <https://doi.org/10.5194/essd-10-985-2018>, 2018.
- Rigby, M. and Western, L.: mrgh/py12box: v0.2.1 (v0.2.1), Zenodo [code], <https://doi.org/10.5281/zenodo.6857447>, 2022a.
- Rigby, M. and Western, L.: py12box\_invert: AGAGE 12-box model inversion (v0.0.2), Zenodo [code], <https://doi.org/10.5281/zenodo.685779>, 2022b.
- Rigby, M., Prinn, R. G., O'Doherty, S., Montzka, S. A., McCulloch, A., Harth, C. M., Mühle, J., Salameh, P. K., Weiss, R. F., Young, D., Simmonds, P. G., Hall, B. D., Dutton, G. S., Nance, D., Mondeel, D. J., Elkins, J. W., Krummel, P. B., Steele, L. P., and Fraser, P. J.: Re-evaluation of the lifetimes of the major CFCs and CH<sub>3</sub>CCl<sub>3</sub> using atmospheric trends, *Atmos. Chem. Phys.*, 13, 2691–2702, <https://doi.org/10.5194/acp-13-2691-2013>, 2013.
- Rigby, M., Prinn, R. G., O'Doherty, S., Miller, B. R., Ivy, D., Mühle, J., Harth, C. M., Salameh, P. K., Arnold, T., Weiss, R. F., Krummel, P. B., Steele, L. P., Fraser, P. J., Young, D., and Simmonds, P. G.: Recent and future trends in synthetic greenhouse gas radiative forcing, *Geophys. Res. Lett.*, 41, 2623–2630, <https://doi.org/10.1002/2013GL059099>, 2014.
- Rigby, M., Park, S., Saito, T., Western, L. M., Redington, A. L., Fang, X., Henne, S., Manning, A. J., Prinn, R. G., Dutton, G. S., Fraser, P. J., Ganesan, A. L., Hall, B. D., Harth, C. M., Kim, J., Kim, K.-R., Krummel, P. B., Lee, T., Li, S., Liang, Q., Lunt, M. F., Montzka, S. A., Mühle, J., O'Doherty, S., Park, M.-K., Reimann, S., Salameh, P. K., Simmonds, P., Tunnicliffe, R. L., Weiss, R. F., Yokouchi, Y., and Young, D.: Increase in CFC-11 emissions from eastern China based on atmospheric observations, *Nature*, 569, 546–550, <https://doi.org/10.1038/s41586-019-1193-4>, 2019.
- Rigby, M., Tunnicliffe, R., Western, L., hanchawn, ag12733, aliceramsden, Jones, G., Young, D., Ward, R., Angharad, ANickless-Bristol, and joe-pitt: ACRG-Bristol/acrg: ACRG v0.2.0 (v0.2.0), Zenodo [code], <https://doi.org/10.5281/zenodo.6834888>, 2022.
- Ruckstuhl, A. F., Henne, S., Reimann, S., Steinbacher, M., Vollmer, M. K., O'Doherty, S., Buchmann, B., and Hueglin, C.: Ro-

- bust extraction of baseline signal of atmospheric trace species using local regression, *Atmos. Meas. Tech.*, 5, 2613–2624, <https://doi.org/10.5194/amt-5-2613-2012>, 2012.
- Salvatier, J., Wiecki, T. V., and Fonnesbeck, C.: Probabilistic programming in Python using PyMC3, *PeerJ Computer Science*, 2, e55, <https://doi.org/10.7717/peerj-cs.55>, 2016.
- Say, D., Ganesan, A. L., Lunt, M. F., Rigby, M., O'Doherty, S., Harth, C., Manning, A. J., Krummel, P. B., and Bauguitte, S.: Emissions of halocarbons from India inferred through atmospheric measurements, *Atmos. Chem. Phys.*, 19, 9865–9885, <https://doi.org/10.5194/acp-19-9865-2019>, 2019.
- Schuck, T. J., Lefrancois, F., Gallmann, F., Wang, D., Jesswein, M., Hoker, J., Bönisch, H., and Engel, A.: Establishing long-term measurements of halocarbons at Taunus Observatory, *Atmos. Chem. Phys.*, 18, 16553–16569, <https://doi.org/10.5194/acp-18-16553-2018>, 2018.
- Simmonds, P. G., Rigby, M., McCulloch, A., O'Doherty, S., Young, D., Mühle, J., Krummel, P. B., Steele, P., Fraser, P. J., Manning, A. J., Weiss, R. F., Salameh, P. K., Harth, C. M., Wang, R. H. J., and Prinn, R. G.: Changing trends and emissions of hydrochlorofluorocarbons (HCFCs) and their hydrofluorocarbon (HFCs) replacements, *Atmos. Chem. Phys.*, 17, 4641–4655, <https://doi.org/10.5194/acp-17-4641-2017>, 2017.
- SPARC: SPARC Report on Lifetimes of Stratospheric Ozone-Depleting Substances, Their Replacements, and Related Species, Tech. Rep., SPARC, <http://www.sparc-climate.org/publications/sparc-reports/> (last access: 14 July 2022), 2013.
- Stohl, A., Seibert, P., Arduini, J., Eckhardt, S., Fraser, P., Grelally, B. R., Lunder, C., Maione, M., Mühle, J., O'Doherty, S., Prinn, R. G., Reimann, S., Saito, T., Schmidbauer, N., Simmonds, P. G., Vollmer, M. K., Weiss, R. F., and Yokouchi, Y.: An analytical inversion method for determining regional and global emissions of greenhouse gases: Sensitivity studies and application to halocarbons, *Atmos. Chem. Phys.*, 9, 1597–1620, <https://doi.org/10.5194/acp-9-1597-2009>, 2009.
- Tang, Y., Lean, H. W., and Bornemann, J.: The benefits of the Met Office variable resolution NWP model for forecasting convection: Variable resolution NWP for forecasting convection, *Meteorol. Appl.*, 20, 417–426, <https://doi.org/10.1002/met.1300>, 2013.
- TEAP: Decisions XXX/3 TEAP Task Force Report on Unexpected Emissions of Trichlorofluoromethane (CFC-11), Tech. Rep., United Nations Environment Programme (UNEP), Nairobi, Kenya, ISBN 978-9966-076-78-6, [https://ozone.unep.org/system/files/documents/TEAP-TF-DecXXX-3-unexpected\\_CFC11\\_emissions-september2019.pdf](https://ozone.unep.org/system/files/documents/TEAP-TF-DecXXX-3-unexpected_CFC11_emissions-september2019.pdf) (last access: 14 July 2022), 2019.
- TEAP: Report of the Technology and Economic Assessment Panel, Volume 1: Progress Report, UN to United Nations, ISBN 978-9966-076-91-5, <https://ozone.unep.org/science/assessment/teap> (last access: 14 July 2022), 2021.
- Trudinger, C. M., Fraser, P. J., Etheridge, D. M., Sturges, W. T., Vollmer, M. K., Rigby, M., Martinerie, P., Mühle, J., Worton, D. R., Krummel, P. B., Steele, L. P., Miller, B. R., Laube, J., Mani, F. S., Rayner, P. J., Harth, C. M., Witrant, E., Blunier, T., Schwander, J., O'Doherty, S., and Battle, M.: Atmospheric abundance and global emissions of perfluorocarbons CF<sub>4</sub>, C<sub>2</sub>F<sub>6</sub> and C<sub>3</sub>F<sub>8</sub> since 1800 inferred from ice core, firn, air archive and in situ measurements, *Atmos. Chem. Phys.*, 16, 11733–11754, <https://doi.org/10.5194/acp-16-11733-2016>, 2016.
- Ul-Haq, Z., Ali, M., Batool, S. A., Tariq, S., and Qayyum, Z.: Emission quantification of refrigerant CFCs, HCFCs and HFCs in megacity Lahore (Pakistan) and contributed ODPs and GWPs, *J. Earth Syst. Sci.*, 125, 1273–1284, <https://doi.org/10.1007/s12040-016-0724-8>, 2016.
- Walters, D. N., Williams, K. D., Boutle, I. A., Bushell, A. C., Edwards, J. M., Field, P. R., Lock, A. P., Morcrette, C. J., Stratton, R. A., Wilkinson, J. M., Willett, M. R., Bellouin, N., Bodas-Salcedo, A., Brooks, M. E., Copsey, D., Earnshaw, P. D., Hardiman, S. C., Harris, C. M., Levine, R. C., MacLachlan, C., Manners, J. C., Martin, G. M., Milton, S. F., Palmer, M. D., Roberts, M. J., Rodríguez, J. M., Tennant, W. J., and Vidale, P. L.: The Met Office Unified Model Global Atmosphere 4.0 and JULES Global Land 4.0 configurations, *Geosci. Model Dev.*, 7, 361–386, <https://doi.org/10.5194/gmd-7-361-2014>, 2014.
- Wan, D., Xu, J., Zhang, J., Tong, X., and Hu, J.: Historical and projected emissions of major halocarbons in China, *Atmos. Environ.*, 43, 5822–5829, <https://doi.org/10.1016/j.atmosenv.2009.07.052>, 2009.
- Wang, Z., Yan, H., Fang, X., Gao, L., Zhai, Z., Hu, J., Zhang, B., and Zhang, J.: Past, present, and future emissions of HCFC-141b in China, *Atmos. Environ.*, 109, 228–233, <https://doi.org/10.1016/j.atmosenv.2015.03.019>, 2015.
- Western, L. M., Ramsden, A. E., Ganesan, A. L., Boesch, H., Parker, R. J., Scarpelli, T. R., Tunnicliffe, R. L., and Rigby, M.: Estimates of North African Methane Emissions from 2010 to 2017 Using GOSAT Observations, *Environ. Sci. Tech. Lett.*, <https://doi.org/10.1021/acs.estlett.1c00327>, 2021.
- Yang, W. and Zurbenko, I.: Kolmogorov–Zurbenko filters, *WIRES Computational Statistics*, 2, 340–351, <https://doi.org/10.1002/wics.71>, 2010.
- Yi, L., Wu, J., An, M., Xu, W., Fang, X., Yao, B., Li, Y., Gao, D., Zhao, X., and Hu, J.: The atmospheric concentrations and emissions of major halocarbons in China during 2009–2019, *Environ. Pollut.*, 284, 117190, <https://doi.org/10.1016/j.envpol.2021.117190>, 2021.
- Zhao, X., Duan, H., and Li, J.: An evaluation on the environmental consequences of residual CFCs from obsolete household refrigerators in China, *Waste Management*, 31, 555–560, <https://doi.org/10.1016/j.wasman.2010.10.018>, 2011.